



HAL
open science

Structure and Mechanism of the Alkyl Hydroperoxidase AhpC, a Key Element of the Mycobacterium tuberculosis Defense System against Oxidative Stress

Beatriz G. Guimarães, Hélène Souchon, Nadine Honoré, Brigitte Saint-Joanis, Roland Brosch, William Shepard, Stewart T. Cole, Pedro M. Alzari

► **To cite this version:**

Beatriz G. Guimarães, Hélène Souchon, Nadine Honoré, Brigitte Saint-Joanis, Roland Brosch, et al.. Structure and Mechanism of the Alkyl Hydroperoxidase AhpC, a Key Element of the Mycobacterium tuberculosis Defense System against Oxidative Stress. *Journal of Biological Chemistry*, 2005, 280 (27), pp.25735-25742. 10.1074/jbc.M503076200 . pasteur-03144583

HAL Id: pasteur-03144583

<https://pasteur.hal.science/pasteur-03144583>

Submitted on 17 Feb 2021

HAL is a multi-disciplinary open access archive for the deposit and dissemination of scientific research documents, whether they are published or not. The documents may come from teaching and research institutions in France or abroad, or from public or private research centers.

L'archive ouverte pluridisciplinaire **HAL**, est destinée au dépôt et à la diffusion de documents scientifiques de niveau recherche, publiés ou non, émanant des établissements d'enseignement et de recherche français ou étrangers, des laboratoires publics ou privés.



Distributed under a Creative Commons Attribution 4.0 International License

Structure and Mechanism of the Alkyl Hydroperoxidase AhpC, a Key Element of the *Mycobacterium tuberculosis* Defense System against Oxidative Stress*

Received for publication, March 21, 2005, and in revised form, May 2, 2005
Published, JBC Papers in Press, May 10, 2005, DOI 10.1074/jbc.M503076200

Beatriz G. Guimarães‡§, Hélène Souchon‡, Nadine Honoré¶, Brigitte Saint-Joanis¶, Roland Brosch¶, William Shepard||, Stewart T. Cole¶, and Pedro M. Alzari‡

From the ‡Unité de Biochimie Structurale, CNRS URA 2185, 25 rue du Docteur Roux and ¶Unité de Génétique Moléculaire Bactérienne, Institut Pasteur, 28 rue du Docteur Roux, 75724 Paris, France and ||European Synchrotron Radiation Facility, 6 rue Jules Horowitz, 38043 Grenoble Cedex, France

The peroxiredoxin AhpC from *Mycobacterium tuberculosis* (MtAhpC) is the foremost element of a NADH-dependent peroxidase and peroxynitrite reductase system, where it directly reduces peroxides and peroxynitrite and is in turn reduced by AhpD and other proteins. Overexpression of MtAhpC in isoniazid-resistant strains of *M. tuberculosis* harboring mutations in the catalase/peroxidase *katG* gene provides antioxidant protection and may substitute for the lost enzyme activities. We report here the crystal structure of oxidized MtAhpC trapped in an intermediate oligomeric state of its catalytic cycle. The overall structure folds into a ring-shaped hexamer of dimers instead of the usual pentamer of dimers observed in other reduced peroxiredoxins. Although the general structure of the functional dimer is similar to that of other 2-Cys peroxiredoxins, the α -helix containing the peroxidatic cysteine Cys⁶¹ undergoes a unique rigid-body movement to allow the formation of the disulfide bridge with the resolving cysteine Cys¹⁷⁴. This conformational rearrangement creates a large internal cavity enclosing the active site, which might be exploited for the design of inhibitors that could block the catalytic cycle. Structural and mutagenesis evidence points to a model for the electron transfer pathway in MtAhpC that accounts for the unusual involvement of three cysteine residues in catalysis and suggests a mechanism by which MtAhpC can specifically interact with different redox partners.

Mycobacterium tuberculosis, the leading cause of death from a single bacterial pathogen, is restrained from proliferation in

most infected individuals by the oxidative and nitrosative stress imposed by the immune response (1). Yet *M. tuberculosis* is able to mount a stubborn antioxidant defense system that allows the pathogen to persist and multiply within the highly oxidative environment of host macrophages (2). This defense system is directly related to mycobacterial drug resistance and virulence. Thus, resistance to isoniazid (INH),¹ a first line anti-tuberculosis agent that inhibits cell wall synthesis after activation by the catalase-peroxidase KatG (3–5), usually arises from mutations in the *katG* gene that result in a protein that is either inactive or has an impaired ability to activate INH (6–8). Although not yet completely defined, the physiological function of KatG includes protection of the mycobacterium against H₂O₂ and other reactive oxygen species produced by the microbe and its host (2, 9). The pathogen needs to compensate the catalase-peroxidase deficiency by alternative peroxidase systems to remain virulent, and several lines of evidence point to the alkyl hydroperoxidase AhpC (MtAhpC) as a key element in fulfilling that role. Thus, enhanced expression of MtAhpC is observed both in INH-resistant KatG-deficient strains (10) as well as in INH-sensitive strains when challenged with the drug (11). Furthermore, the saprophytic *Mycobacterium smegmatis*, naturally insensitive to INH, shows a dramatic increase of INH susceptibility after insertional inactivation of the *ahpC* gene (11).

MtAhpC is a member of a large family of peroxidases, the peroxiredoxins, found in most living organisms. Peroxiredoxins are responsible for the antioxidant defense in bacteria, yeast, and trypanosomatids; they participate in balancing hydroperoxide production during photosynthesis in plants and appear to control cytokine-induced peroxide levels that mediate signal transduction in mammalian cells (see Refs. 12 and 13 for recent reviews). In mycobacteria, AhpC can not only detoxify hydroperoxides but also affords protection to cells against reactive nitrogen intermediates (14, 15). MtAhpC specifically catalyzes the conversion of peroxynitrite (OONO⁻) to nitrite fast enough to avoid the spontaneous decomposition of the former into the deleterious nitrogen dioxide and hydroxyl radicals (16). The NADH-dependent peroxidase and peroxynitrite reductase system of *M. tuberculosis* involves MtAhpC as the foremost element of a chain that also includes the MtAhpC-reducing protein, AhpD, dihydroliipoamide dehydrogenase, Lpd, and dihydroliipoamide succinyltransferase, SucB (17), although alter-

* This work was supported in part by grants from the Institut Pasteur (GPH-5), the Ministry of Research (Contract 01-B-0095), the European Union (X-TB, Contract QLK2-CT-2001-02018, and SPINE, Contract QLG2-CT-2002-00988), and the National Genopole Network, France (Contract RNG-2002-008). The costs of publication of this article were defrayed in part by the payment of page charges. This article must therefore be hereby marked "advertisement" in accordance with 18 U.S.C. Section 1734 solely to indicate this fact.

The atomic coordinates and structure factors (code 2BMX) have been deposited in the Protein Data Bank, Research Collaboratory for Structural Bioinformatics, Rutgers University, New Brunswick, NJ (<http://www.rcsb.org/>).

§ Recipient of a fellowship from Fundação de Amparo à Pesquisa do Estado de São Paulo (FAPESP) (Brazil). Present address: Centro de Biologia Molecular Estrutural, Laboratório Nacional de Luz Síncrotron, Caixa Postal 6192, CEP 13084-971, Campinas, Sao Paulo, Brasil.

** To whom correspondence should be addressed: Unité de Biochimie Structurale, Institut Pasteur, 25 rue du Docteur Roux, 75724 Paris Cedex 15, France. Tel.: 33-145688607; Fax: 33-145688604; E-mail: alzari@pasteur.fr.

¹ The abbreviations used are: INH, isoniazid; MtAhpC, AhpC from *Mycobacterium tuberculosis*; SeMet, selenomethionine; StAhpC, *Salmonella typhimurium* AhpC; Tpx-B, thioredoxin peroxidase B; MAD, multiwavelength anomalous diffraction phasing; SAD, single wavelength anomalous diffraction.

native thioredoxin-mediated pathways including MtAhpC have also been reported (18).

Peroxiredoxins (EC 1.11.1.15) use redox-active cysteine residues to reduce their substrates and can be classified into three classes (typical 2-Cys, atypical 2-Cys, and 1-Cys enzymes) based on the number and the sequence positions of cysteinyl residues involved in catalysis (13). In all three classes, the first step of the peroxidase reaction involves a conserved N-terminal cysteine (the peroxidatic cysteine), which attacks the peroxide/peroxynitrite substrate and is oxidized to a cysteine sulfenic acid (Cys-SOH). Typical 2-Cys peroxiredoxins like MtAhpC are obligate homodimers in which the second (C-terminal) cysteine from one subunit acts as the resolving cysteine to attack the peroxidatic cysteine sulfenic acid located in the other subunit. The ensuing condensation reaction results in the formation of a stable intersubunit disulfide bond, which is then reduced by one of several cell-specific disulfide oxidoreductases, completing the catalytic cycle.

Although MtAhpC is usually considered a typical 2-Cys peroxiredoxin, it differs in a number of important features from other members of the family. First, MtAhpC has three (rather than two) cysteine residues directly involved in catalysis (19), the conserved peroxidatic cysteine Cys⁶¹, the putative resolving cysteine Cys¹⁷⁴, and a third cysteine, Cys¹⁷⁶, whose catalytic role is unclear (20, 21). Second, it remained an enigma how MtAhpC is supplied with reduction equivalents because the thioredoxin system that reduces peroxiredoxins in eukaryotic H₂O₂ metabolism was reported to be inactive as a reductant of MtAhpC (19), and there is no homologue in the mycobacterial genome of the AhpF flavoprotein known to reduce AhpC in *Salmonella typhimurium* (22). Instead, MtAhpC is reduced by a novel atypical system involving AhpD (17), a thioredoxin-like protein that is only found in a restricted number of organisms.

Here, we report the 2.4-Å structure of the C176S point mutant of MtAhpC trapped in an intermediate state of its catalytic cycle. The functional dimer of MtAhpC_{C176S} has a structure similar to those of other 2-Cys peroxiredoxins. However, although the oxidized protein behaves as a dimer in solution, it crystallized in an oligomeric (12-mer) form resembling the decameric forms observed for other peroxiredoxins (12, 13). In agreement with available mutagenesis data, the structure suggests a model for the peroxidase reaction that can explain the involvement of the three cysteine residues in catalysis. To facilitate the formation of the Cys⁶¹-Cys¹⁷⁴ disulfide bond, the entire α -helix containing the peroxidatic cysteine is seen to undergo a rigid-body displacement instead of the partial helical unwinding observed in the disulfide-bonded forms of other 2-Cys peroxiredoxins (13). This unusual movement generates a large internal cavity, which encloses the reaction center and might provide a structural framework for the design of inhibitors with potential therapeutic applications.

MATERIALS AND METHODS

Cloning and Site-directed Mutagenesis—PCR amplification of the *ahpC* gene was performed using primers *ahpC*-2726F CCCGGTCTCCATGCCACTGCTAACCATT and *ahpC*-2727R TTCCCGCCATGGAGATCCCGGTT into which a BsaI site or a NcoI site were introduced. After digestion of the PCR product with BsaI and NcoI, the fragment was ligated into NcoI-digested pET16b (Novagen), electroporated into XL2 blue cells, and plated out on ampicillin-containing plates (100 μ g/ml). Plasmid DNA was prepared from several colonies using standard methods, and correct insertion of the fragment into the vector was controlled by sequencing. Overexpression of MtAhpC was then performed in strain BL21.

The *ahpC*-containing pET16b plasmid was then subjected to mutagenesis using the chameleon kit (Stratagene) following the manufacturer's instructions to produce a single mutant (C176S) and a double mutant (C174S,C176S) of MtAhpC. To achieve the replacement of se-

lected bases, the primer SP2, GACTTGTTGACGCGTACCAGTCAC, was used together with either the primer GCGCCAGTTGCTTGCGCAGAGCT to produce the single Cys mutant or with the primer GCCAGTTGCTTGCGCTCAGCTCGTC to produce the double mutant.

Protein Expression and Purification—Wild-type MtAhpC and the mutants MtAhpC_{C176S} and MtAhpC_{C174S,C176S} were produced following a similar protocol. *Escherichia coli* BL21 cells were cultured in ampicillin-supplemented LB medium, induced at mid-log phase with 1 mM isopropyl 1-thio- β -D-galactopyranoside and grown overnight at 20 °C. The culture was harvested by centrifugation and resuspended in a buffer containing 50 mM potassium phosphate, pH 7.5, and a protease inhibitor mixture (Roche Applied Science). Cells were disrupted in a French press and centrifuged at 17,000 \times g for 30 min. The supernatant was treated with streptomycin sulfate (w/w ratio of 1/1), gently stirred for 45 min at 4 °C, and fractionated with ammonium sulfate at 50 and 70% saturation. The final precipitate was dissolved, dialyzed against 50 mM potassium phosphate, pH 7.5, and loaded onto a DEAE column equilibrated with the same buffer. The purified protein was eluted at 0.1 M potassium chloride and concentrated to 16 mg/ml by ultrafiltration in 20 mM Tris-HCl, pH 7.5, for use in crystallization assays.

For MtAhpC_{C176S}, the selenomethionine (SeMet)-labeled protein was expressed in the non-methionine auxotroph *E. coli* strain BL21(DE3) following protocols described previously (23). Briefly, cells were cultured in M9 minimal medium containing glucose (0.4% w/v) and ampicillin (100 mg/liter). Amino acids lysine, threonine, and phenylalanine (100 mg/liter), leucine, isoleucine, and valine (50 mg/liter) together with SeMet (50 mg/liter) were added as solids 30 min before induction. AhpC expression was induced at mid-log phase with 1 mM isopropyl 1-thio- β -D-galactopyranoside, and cell growth was continued overnight at 20 °C. The SeMet-labeled protein was purified following the same protocol described above for non-labeled proteins, and SeMet incorporation was confirmed by mass spectrometry (not shown).

Analytical gel filtration experiments were carried out on a SMART high pressure liquid chromatography system (Amersham Biosciences) using a Superdex-200 column equilibrated in 50 mM potassium phosphate, pH 7.0, 100 mM potassium chloride, 1 mM EDTA, and 2% glycerol. The proteins were eluted under reducing (10 mM dithiothreitol) or non-reducing conditions using a flow rate of 40 μ l/min and were monitored at 280 nm.

Crystallization and Data Collection—Crystallization trials were performed at 18 °C using the hanging drop vapor diffusion method. The best crystals of MtAhpC_{C176S} (either unlabeled or SeMet-labeled protein) reached a size of 0.2 \times 0.2 \times 0.4 mm and were obtained from drops made of 2–4 μ l of protein solution (16 mg/ml) mixed with an equal volume of a reservoir solution containing 0.1 M sodium citrate, pH 6.0, 16% ammonium sulfate. Crystals were frozen in liquid nitrogen in the presence of a cryoprotectant solution (the same mother liquor with 30% glycerol) for data collection. Extensive crystallization assays were also carried out with wild-type AhpC and the double mutant AhpC_{C174S,C176S}, but these attempts systematically resulted in microcrystals unsuitable for x-ray diffraction studies.

X-ray diffraction data sets were collected at 110°K using synchrotron radiation (European Synchrotron Radiation Facility, Grenoble, France). For multiwavelength anomalous diffraction phasing (MAD), four data sets of the SeMet-labeled protein were collected at 2.5 Å resolution on the ID29 beamline at different wavelengths (peak, inflection point, and two remote wavelengths) derived from a scan of the selenium K absorption edge. Using another crystal, a separate, highly redundant data set was collected at a single wavelength corresponding to the largest value for the anomalous difference f'' . All data were processed using the programs MOSFLM, SCALA, and TRUNCATE from the CCP4 package (24). The crystals belong to space group P622 and contain three monomers per asymmetric unit, with a large (62%) solvent fraction. Unit cell dimensions and data collection statistics are shown in Table I.

Structure Determination and Refinement—The structure of MtAhpC_{C176S} was determined by a MAD experiment after molecular replacement calculations with known dimeric and decameric structures of 2-Cys peroxiredoxins proved unsuccessful. The three selenium sites (one per monomer) were found by Patterson methods and their atomic positions, B-factors, and occupancies refined with the program SHARP (25). Despite the low content of anomalous scatterers (one selenium atom in 195 protein residues), experimental phases could be calculated to 2.6-Å resolution with an overall figure-of-merit of 0.65 (0.81 after density modification) and resulted in a readily interpretable electron density map.

Chain tracing was carried out with the program O (26). Most α -helices and all β -sheets were well defined in density, and a total of 137

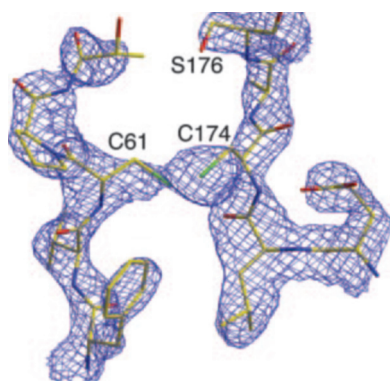


FIG. 1. Electron density map calculated with SAD phases (contoured at 1.5 σ) showing the disulfide bond between Cys⁶¹ from monomer A and Cys¹⁷⁴ from monomer B. The final model is shown superimposed.

residues in each of the three subunits could be independently modeled using the positions of the anomalous scatterers and large aromatic residues as markers. However, the C-terminal region including the resolving cysteine Cys¹⁷⁴, two protein loops, and the α -helix containing the peroxidatic cysteine Cys⁶¹ were poorly defined in the experimental map, and the situation did not improve significantly after initial refinement cycles with the program REFMAC (27) from the CCP4 package.

At this stage, we decided to collect a highly redundant data set from another SeMet-labeled crystal at a single wavelength corresponding to the f' peak (Table I). After SHARP phasing, experimental phases were calculated to 2.4-Å resolution with an overall figure-of-merit of 0.50 and 0.81 before and after density modification, respectively, and the resulting electron density map unambiguously showed a disulfide bridge involving the peroxidatic cysteine from one of the monomers (Fig. 1). Crystallographic refinement was carried out against the SAD data set at 2.4-Å resolution using the program REFMAC, alternating with visual inspection of the electron density maps and model rebuilding with the program O. During the final cycles water molecules were introduced using the program ARP/wARP (28). The final model (Protein Data Bank accession code 2BMX) has an R -factor of 0.195 ($R_{\text{free}} = 0.236$) to 2.4-Å resolution. Further details of refinement are presented in Table II.

Quality of the Model—The final atomic model of MtAhpC_{C176S} includes three crystallographically independent monomers (labeled A–C) and 284 water molecules. The quality of the electron density allowed modeling of amino acid residues 2–170 (of 195) in monomers A and C and amino acid residues 2 to 179 in monomer B. The α -helix that follows the N-terminal peroxidatic cysteine Cys⁶¹ is partially disordered in monomers B and C, and in all three monomers the loop formed by residues 21–31 is largely exposed to solvent and poorly defined in the electron density map. The final model displays a good overall stereochemistry. As defined by the program PROCHECK (29), all non-glycine and non-proline residues display main-chain dihedral angles that fall within the most favored or additionally allowed regions of the Ramachandran plot.

The crystal packing consists of successive layers of dodecamers in the (x, y) plane centered on the crystallographic 6-fold axis. Two of the three independent monomers (A and B, at $z = 1/3$) are associated into a non-crystallographic dimer, whereas the third monomer (at $z = 0$) forms a crystallographic dimer. The overall root mean square deviations for 168 C α positions between crystallographically independent monomers are 0.38 Å (A and B), 0.59 Å (A–C), and 0.41 Å (B and C). The two non-equivalent dodecamers (at $z = 0$ and $z = 1/3$) are related to each other by a rotation of 11° around the crystallographic z -axis, which might explain the difficulties encountered in determining this crystal structure using molecular replacement methods.

RESULTS AND DISCUSSION

Solution Studies—The amino acid sequence of MtAhpC contains three cysteines at positions 61, 174, and 176, all of which are directly involved in catalysis (19, 20). The N-terminal cysteine, Cys⁶¹, is strictly conserved in all peroxiredoxins and serves as the peroxidatic cysteine to carry out the initial attack on the peroxide substrates, whereas Cys¹⁷⁴ was also shown to be crucial for catalysis and probably acts as the resolving cysteine. For our structural studies, we therefore produced

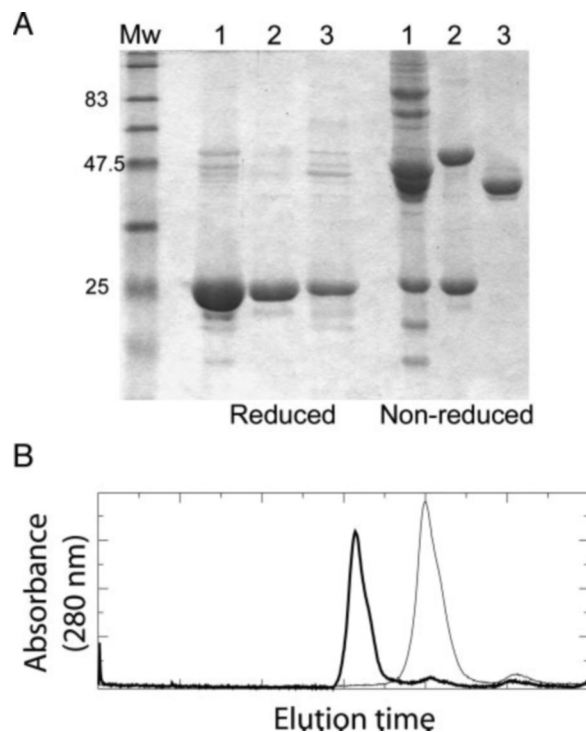


FIG. 2. Redox-dependent oligomerization of MtAhpC. A, SDS-PAGE of wild-type MtAhpC (lane 1), the double mutant MtAhpC_{C174S,C176S} (lane 2), and the single mutant MtAhpC_{C176S} (lane 3). Mw, molecular weight. B, gel filtration elution profiles of purified MtAhpC_{C176S} in the absence (thin line) and presence (thick line) of 10 mM dithiothreitol.

wild-type MtAhpC, the single point mutant MtAhpC_{C176S} that might retain the mode of action of 2-Cys peroxiredoxins, and the double mutant MtAhpC_{C174S,C176S} (maintaining only the critical peroxidatic cysteine) as recombinant proteins in *E. coli*. SDS-PAGE experiments of these proteins under reducing and non-reducing conditions revealed the role of disulfide bonds in protein aggregation (Fig. 2A). In our hands, wild-type MtAhpC appeared as multiple bands in SDS-PAGE under non-reducing conditions, different from what has been observed by other authors (19, 20). The protein migrated primarily as a dimer under non-reducing conditions, indicating the formation of an intersubunit disulfide bridge (probably between Cys⁶¹ and Cys¹⁷⁴ or Cys¹⁷⁶). However, the presence of higher oligomers indicated that the third cysteine is highly reactive and readily involved in nonspecific intermolecular disulfide bonds. On the other hand, the double mutant MtAhpC_{C174S,C176S} showed the presence of covalent dimers that disappeared under reducing conditions, implying that Cys⁶¹ is involved in nonspecific intermolecular disulfide bridges. Instead, the mutant MtAhpC_{C176S} migrated as a single molecular species corresponding to the dimeric form under non-reducing conditions, thus demonstrating that the protein is fully oxidized under the experimental conditions used and making this mutant the best candidate for crystallization studies.

In agreement with the above results, size exclusion chromatography showed significant differences between the elution profiles of wild-type MtAhpC and the single point mutant MtAhpC_{C176S} under non-reducing and reducing conditions. Wild-type MtAhpC behaves as a heterogeneous mixture of oligomers under non-reducing conditions, whereas in the presence of 10 mM dithiothreitol the elution profile changes into a homogeneous species corresponding to a 10- or 12-mer (data not shown). In contrast, MtAhpC_{C176S} elutes as a single oligomeric species under both reducing and non-reducing conditions

TABLE I
Data collection statistics

Data set	MAD				SAD
	Peak	Inflection	Remote 1	Remote 2	
Wavelength (Å)	0.9796	0.9797	0.9611	0.9184	0.9793
Cell dimensions (Å)	$a = b = 139.6$ $c = 148.9$	$a = b = 139.7$ $c = 149.1$	$a = b = 139.8$ $c = 149.2$	$a = b = 140.0$ $c = 149.4$	$a = b = 139.3$ $c = 148.5$
Resolution range (Å)	30–2.5	30–2.5	30–2.5	30–2.5	30–2.4
(outermost shell) (Å)	(2.64–2.5)	(2.64–2.5)	(2.64–2.5)	(2.64–2.5)	(2.53–2.4)
Unique reflections	30162	30252	30313	30381	33798
Multiplicity	10.3 (10.6)	10.3 (10.6)	10.3 (10.6)	10.3 (10.6)	31.3 (31.2)
Completeness (%)	99.8 (99.8)	99.8 (99.8)	99.8 (99.8)	99.8 (99.8)	99.9 (99.9)
R_{sym} (%)	5.9 (25.9)	5.9 (28.8)	6.2 (33.6)	6.5 (36.7)	8.2 (39)
$I/\sigma(I)$	9.9 (2.8)	10.0 (2.6)	9.6 (2.5)	8.9 (2.0)	6.5 (1.9)
R_{anom} (%)	3.2 (8.5)	2.2 (9.1)	2.5 (10.8)	2.4 (12.4)	2.8 (7.4)

(Fig. 2B). In its oxidized state, the protein behaves as a dimer, which oligomerizes to form a 10- or 12-mer upon the addition of 10 mM dithiothreitol. These experiments demonstrate that the reduced state of the protein is associated with a higher oligomeric form, a hypothesis put forward by Alpey *et al.* (30) from their structural studies of the reduced tryparedoxin peroxidase TryP from *Crithidia fasciculata* and now verified for other members of this family (13).

The Crystal Structure of MtAhpC—The structure of MtAhpC_{C176S} in its oxidized state was determined by a MAD experiment at four different wavelengths (Table I) and refined to a final R -factor of 0.195 ($R_{\text{free}} = 0.236$) (Table II). In the crystal, MtAhpC_{C176S} associates to form a ring-shaped 12-mer with an outer diameter of 140 Å and an inner diameter of 70 Å (Fig. 3A). Formation of a 12-mer was unexpected for two reasons: first, because all peroxiredoxins structurally characterized to date as oligomers had revealed a decameric form, and second, because the oxidized protein behaves as a dimer in solution (Fig. 2B). This last observation implies that the protein is trapped in an intermediate state of its catalytic cycle, probably stabilized by crystal contacts, in which the condensation reaction has taken place but the oligomeric form has not yet disassembled into the functional dimer. A similar intermediate has been observed previously for *S. typhimurium* AhpC (StAhpC) (31), where it was also proposed that crystal packing forces help to stabilize the oligomeric form of the protein.

More puzzling is the observation that MtAhpC consists of a hexamer of dimers, rather than the expected pentamer of dimers observed in other homologues such as TryP (30), StAhpC (31), and human thioredoxin peroxidase B (Tpx-B) (32). Indeed, several lines of evidence tend to indicate that formation of 10-mers may be a general property of 2-Cys peroxiredoxins in which the oligomeric form is associated with the reduced enzyme (13). For MtAhpC, recent studies using cross-linking and gel filtration experiments showed that the protein is a 10-mer (or 12-mer) that disassembles to form dimers at high ionic strength (33), and we show now for the point mutant MtAhpC_{C176S} that these changes in oligomerization are also associated with the redox state of the protein (Fig. 2B). As gel filtration experiments cannot differentiate between the 10-mer and 12-mer forms of the reduced protein in solution, we carried out analytical sedimentation, small-angle x-ray scattering, and preliminary electron microscopy experiments in an attempt to discriminate between the two forms. However, the results were not conclusive. Although a 10-mer model appears to fit slightly better the experimental small-angle x-ray scattering profile (data not shown), it was impossible to unambiguously identify the oligomeric form of MtAhpC from these experiments.

Dimer-dimer interactions in the crystal structure of 12-mer MtAhpC bury 1440 Å² of molecular surface. As in 10-mer peroxiredoxins, the character of this interface is largely hydrophobic, including residues Phe⁵⁷, Thr⁵⁸, Phe⁹¹, Ile¹¹⁴, and

TABLE II
Refinement statistics

Resolution range (Å)	30–2.4
Reflections used	32082
R -factor ^a	0.195
Free R -factor ^b	0.236
r.m.s. ^c deviations from ideality	
Lengths (Å)	0.020
Angles (°)	1.82
Protein atoms (B_{avg} , Å ²)	3963 (40.4)
Water molecules (B_{avg} , Å ²)	284 (41.9)

^a R -factor = $\sum_{hkl} |F_{\text{obs}}| - k [F_{\text{calc}}] / \sum_{hkl} |F_{\text{obs}}(hkl)|$.

^b calculated as R -factor for 5% of the total data not used in refinement.

^c r.m.s., root mean square.

Val¹³⁰ and the aliphatic moieties of Lys⁵⁵, Gln⁹⁵, and Lys¹¹⁵ from each interacting monomer. Adjacent dimers in MtAhpC also interact through four intermolecular hydrogen bonds connecting the Lys¹¹⁵ and Arg¹¹⁶ side chains with the main-chain carboxyl groups in the other monomer and two salt bridges between Lys⁵⁵ and Glu⁹⁰. Despite their distinct mode of oligomerization, the dimer-dimer interface in 12-mer MtAhpC is very similar to that observed in 10-mer peroxiredoxins (Fig. 3B). In particular, two conserved residues (Phe⁵⁷ and Trp⁹⁶, MtAhpC numbering), for which a reorientation of their side chains is directly associated with the redox-induced dimer-decamer switch in peroxiredoxins (30, 32), display the same conformation in the 12-mer and 10-mer structures, suggesting that a similar redox-induced switch may also be operational in MtAhpC (Fig. 2B). These close similarities strongly suggest that the observed MtAhpC oligomer, although stabilized by crystal forces, probably corresponds to a functionally relevant form of the (reduced) protein in solution.

The Functional Dimer—The functional MtAhpC dimer (Fig. 3B) is similar to those of other 2-Cys enzymes with an overall ellipsoidal shape of approximate dimensions 85 × 35 × 35 Å. The core of each monomer comprises a thioredoxin-like fold composed of a central β -sheet (strands $\beta 6$, $\beta 5$, $\beta 8$, $\beta 9$) and three flanking α -helices ($\alpha 1$, $\alpha 3$, $\alpha 4$) with additional insertions at the N terminus (strands $\beta 1$ – $\beta 4$) and between $\beta 6$ and $\alpha 3$ (helix $\alpha 2$ and strand $\beta 7$). A long loop (residues 21–31 connecting strands $\beta 3$ and $\beta 4$), absent in other peroxiredoxins of known three-dimensional structure, is highly flexible and poorly defined in the electron density map of MtAhpC. As in typical 2-Cys peroxiredoxins, the dimer interface is created by the interaction of the two thioredoxin-like cores, involving the formation of an extended intermolecular β -sheet, as well as additional contacts made by the $\beta 9$ - $\alpha 4$ connecting loop and the N- and C-terminal tails.

The three critical cysteine residues (Cys⁶¹, Cys¹⁷⁴, and Cys¹⁷⁶) of MtAhpC are clustered together at the molecular surface (Fig. 3B), with the first two engaged in the disulfide

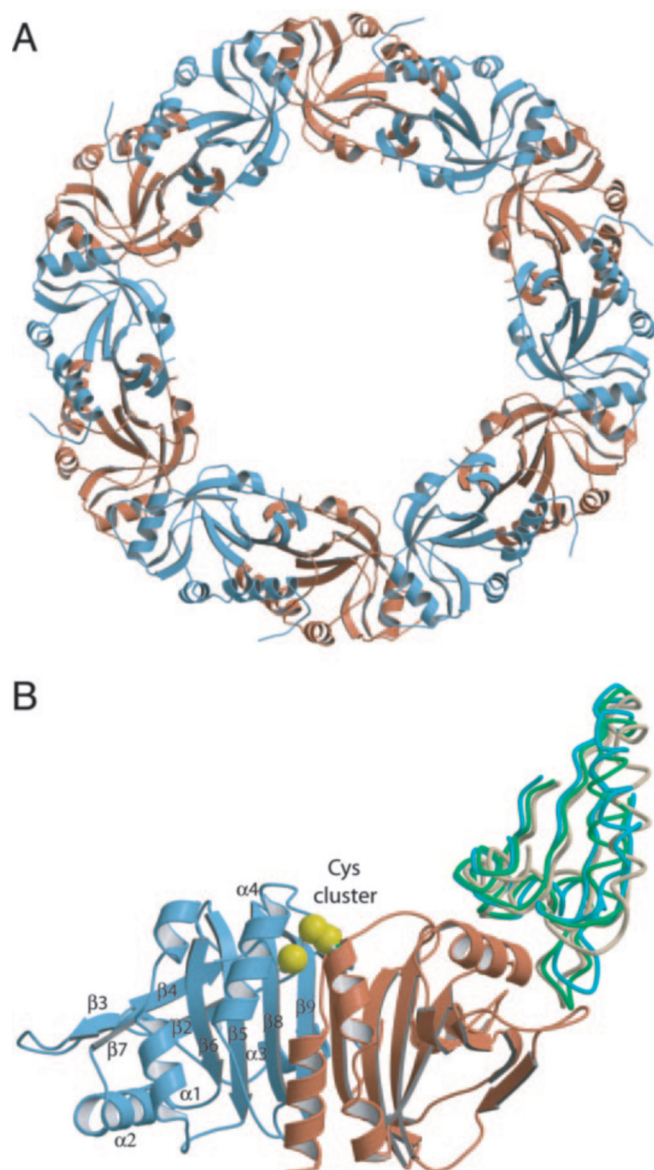


FIG. 3. Overall view of the MtAhpC_{C176S} structure. A, the oligomeric structure as seen in the crystal. B, structure of the functional MtAhpC dimer in ribbon representation. The position of the three catalytic cysteine residues is shown for one of the monomers (Ser¹⁷⁶ in the crystal structure was replaced by wild-type Cys¹⁷⁶), and the numbering of secondary structure elements is shown for the second monomer. Also shown is the position of the adjacent monomer in oligomeric peroxiredoxins, indicating a conserved dimer-dimer interface in 10- and 12-mer enzymes. After least squares superposition of the functional dimer, the adjacent monomer is shown for MtAhpC (12-mer, cyan), human TPx-B (10-mer, green), and StAhpC (10-mer, brown). The figure was prepared using MOLSCRIPT (38) and RASTER3D (39).

bridge conserved in typical 2-Cys peroxiredoxins. In the structure of the point mutant MtAhpC_{C176S}, the intermolecular disulfide is well defined in the electron density map only for Cys⁶¹ from monomer A and Cys¹⁷⁴ from monomer B (Fig. 1). However, a rigid-body movement of helix $\alpha 1$ that is required for disulfide bond formation (see below) is observed in the three crystallographically independent monomers, strongly suggesting that the protein is entirely oxidized in the crystal, in agreement with the SDS-PAGE data (Fig. 2A). This oxidized form represents an intermediate of the peroxidation reaction catalyzed by 2-Cys peroxiredoxins and was observed in the structures of *Rattus norvegicus* 2-Cys peroxiredoxin HBP23 (34) and StAhpC (31). Although the disulfide bond is buried and sur-

rounded by several hydrophobic residues in the HBP23 structure, in MtAhpC it is largely exposed to the solvent, and its hydrophobic environment is less pronounced. The Cys⁶¹–Cys¹⁷⁴ bond is surrounded by the hydrophobic side chains of Phe⁵⁹(A), Pro⁶²(A), and Leu¹⁷³(B), the charged residues Glu¹⁷²(B) and Asn¹⁷⁷(B), and the polar residues Thr⁶³(A) and Ser/Cys¹⁷⁶(B).

Peroxide decomposition likely requires a base to deprotonate the peroxidatic cysteine as well as an acid to protonate the poor RO leaving group, although these catalysts have yet to be identified. The competent active site of MtAhpC cannot be analyzed from the crystal structure because the protein has been trapped in an intermediate state of the reaction after peroxide reduction by Cys⁶¹ and the condensation reaction with Cys¹⁷⁴. However, the critical active site residues found in other peroxiredoxins (13), in particular Pro⁵⁴, Thr⁵⁸, and Arg¹³³, are also conserved in the mycobacterial enzyme and are expected to adopt a similar conformation at the beginning of the reaction.

Conformational Flexibility of Helix $\alpha 1$ —In typical 2-Cys peroxiredoxins, the sulfenic acid at the peroxidatic cysteine (formed upon peroxide reduction as seen in the crystal structure of the human 1-Cys peroxiredoxin hORF6 (35)) is attacked by the C-terminal resolving cysteine from the other monomer to form an intermolecular disulfide bond. This condensation reaction requires significant conformational changes both in helix $\alpha 1$, in which the helical portion of the loop-helix active-site motif is unwound to expose the peroxidatic cysteine (13), and in the C-terminal arm to correctly position the resolving cysteine for disulfide bond formation. This linkage is observed in the dimeric structure of (oxidized) HBP23, whereas in the decameric structures of TPx-B and TryP the S γ atoms from the two Cys residues are about 10 Å apart from each other. A third situation is observed in the structures of the StAhpC and MtAhpC reaction intermediates, in which the condensation reaction has taken place but the oligomers have not yet disassembled. However, the nature of the MtAhpC intermediate is significantly different (Fig. 4A). Instead of the local unwinding of helix $\alpha 1$ observed in known oxidized structures (including the StAhpC intermediate) to render accessible the peroxidatic cysteine for disulfide formation, this is achieved in MtAhpC by a rigid-body movement of the entire helix that brings Cys⁶¹ close to Cys¹⁷⁴. This movement does not appear to be forced by the molecular packing in the crystal because it is not observed in decameric StAhpC, which has a very similar dimer-dimer interface (Fig. 3B) and in which the oligomeric arrangement is also stabilized by crystal packing forces.

The above observations strongly suggest that the helical displacement is directly related to the MtAhpC mechanism of action. A rigid-body movement of the helix can position the peroxidatic cysteine (Cys⁶¹) either in contact with the resolving cysteine (Cys¹⁷⁴), as seen in the crystal structure, or back to the active center upon disruption of the disulfide bridge, in which case the position of the helix would coincide with that observed in the other peroxiredoxin structures (Fig. 4). No major conformational changes are required for this movement to occur, except for a small rearrangement of three phenylalanine side chains (Phe⁵¹, Phe⁶⁸, Phe¹⁰⁸). Such a helical displacement would position Cys⁶¹ at H-bonding distance of Arg¹³³ and the carboxylate group of Glu⁶⁴ in contact with the guanidinium groups of both Arg¹³³ and Arg¹⁵⁶, thus reconstituting a competent active site for peroxide reduction.

Implications for Structure-based Drug Design—The MtAhpC/AhpD peroxidase system appears to play an important role in *M. tuberculosis* resistance against the oxidative and nitrosative stress exerted by the host immune response (17). These enzymes may thus represent suitable targets for novel

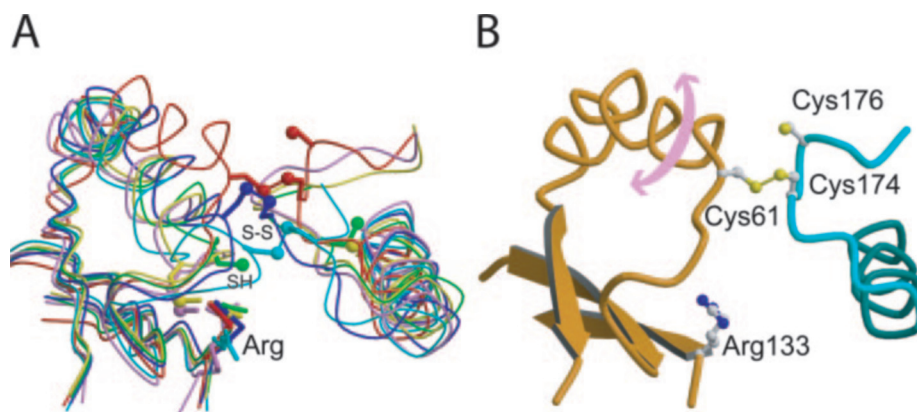


FIG. 4. **Conformational rearrangement of helix $\alpha 1$ in MtAhpC.** A, superposition of selected regions from MtAhpC (red), StAhpC (blue), HBP23 (cyan), human TPx-B (yellow), hORF6 (violet), and TryP (green). The side chains of the two catalytic Cys residues and the conserved arginine residue (MtAhpC-Arg¹³³) in the active site are shown; secondary structure elements are labeled as in Fig. 3. Note the different position of helix $\alpha 1$ in MtAhpC. B, same view for MtAhpC alone. A rigid-body movement of helix $\alpha 1$ (arrow) would allow the peroxidatic cysteine (Cys⁶¹) to be in contact with the two resolving cysteines (Cys¹⁷⁴ or Cys¹⁷⁶) or to restore a competent active site, with Cys⁶¹ close to Arg¹³³ and helix $\alpha 1$ positioned as in the other peroxiredoxin structures.

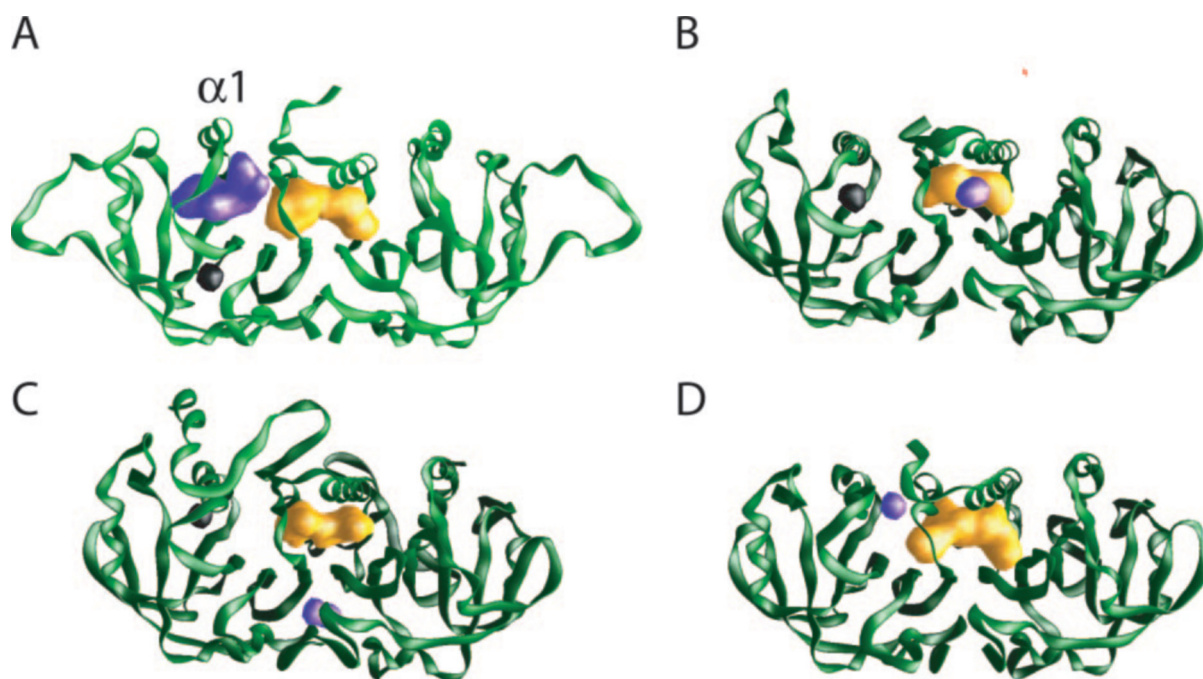


FIG. 5. **Internal cavities in the crystal structures of various peroxiredoxins.** A, MtAhpC; B, TryP; C, TPx-B; and D, HBP23. The movement of helix $\alpha 1$ in MtAhpC (labeled) generates a new internal cavity that is absent in other peroxiredoxins.

antituberculosis strategies, in particular for INH-resistant *M. tuberculosis* strains where MtAhpC is thought to compensate for the decreased catalase-peroxidase KatG activity (15, 16). However, a potent AhpD inhibitor was recently found to be unable to suppress the growth of INH-resistant *M. tuberculosis* in infected mouse lungs (36). Koshkin *et al.* (36) argue that a low titer of AhpD may still suffice to maintain MtAhpC activity, reinforcing the hypothesis that the latter is the right target for drug design against this detoxification system. The crystal structure of MtAhpC now reveals that the movement of helix $\alpha 1$ generates a cavity, which is missing in other peroxiredoxin structures (Fig. 5) and might provide a putative platform for drug design. If the helical movement does indeed occur during the normal catalytic cycle as proposed above, a compound that fits into this pocket could block the enzyme in its intermediate state by precluding completion of the catalytic cycle. More importantly, the enzyme could thus be specifically inhibited without directly interfering with the catalytic center, which is largely conserved within the peroxiredoxin family.

The Catalytic Cycle of MtAhpC and the Involvement of Three Cys Residues in Catalysis—A detailed model of the peroxiredoxin catalytic cycle has emerged from available structural and biochemical evidence (13, 31), although in the case of MtAhpC different reaction mechanisms engaging the three catalytic cysteines may be envisaged to account for its sequential reduction by the redox partner. After peroxide reduction, the peroxidatic cysteine in helix $\alpha 1$ changes to sulfenic acid (SOH), which is in turn attacked by the sulfhydryl group of the resolving cysteine, either Cys¹⁷⁴ or less commonly Cys¹⁷⁶. This mechanism is supported by mutagenesis studies of MtAhpC showing that both Cys⁶¹ and Cys¹⁷⁴ (but not Cys¹⁷⁶) appear to be crucial for activity (20) and that Cys¹⁷⁶ is able to partially substitute for Cys¹⁷⁴ in the C174S mutant (21). Indeed, this redundancy in the roles of Cys¹⁷⁴ and Cys¹⁷⁶ as resolving cysteines could be accounted for by the rigid-body movement of helix $\alpha 1$, which can easily bring Cys⁶¹ close to either Cys¹⁷⁴ (as in the crystal structure) or Cys¹⁷⁶ (see Fig. 4B).

Once the condensation reaction has taken place, in typical

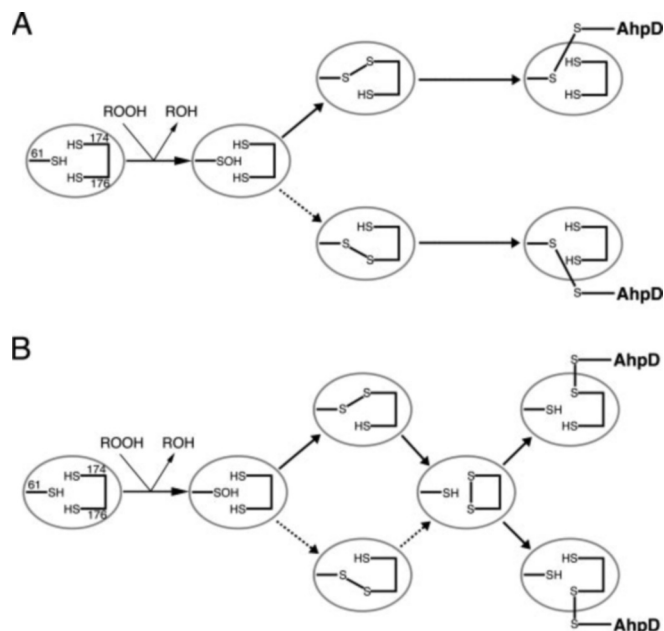


FIG. 6. Possible reaction mechanisms for the sequential reduction of MtAhpC by AhpD. A, mechanism proposed in Ref. 21. B, alternative mechanism involving an intermediate disulfide bridge between Cys¹⁷⁴ and Cys¹⁷⁶.

2-Cys peroxiredoxins a direct attack by an external thiol is thought to reduce the disulfide. From their studies on the formation of reversible covalent MtAhpC/AhpD adducts, Koshkin *et al.* (21) also favored such a mechanism for MtAhpC. According to these authors, the SH group of AhpD-Cys¹³³³ would attack the Cys⁶¹-Cys¹⁷⁴ bond to form an intermolecular Cys¹³³³-Cys⁶¹ adduct (Fig. 6A). It should be emphasized that, for such a mechanism to occur, the two proteins must undergo significant conformational rearrangements, given the internal positions of the cysteine residues in the corresponding crystal structures of MtAhpC (this work) and AhpD (17, 37).

The structure of MtAhpC_{C176S} now suggests an alternative possibility involving the participation of the three cysteine residues in catalysis. In the crystal structure, the O γ atom of Ser¹⁷⁶ (which substitutes for Cys¹⁷⁶ in the wild-type enzyme) is distant 4.9 and 5.5 Å from the S γ atoms of Cys¹⁷⁴ and Cys⁶¹, respectively. Therefore, the hypothesis of a second intramolecular disulfide bond involving Cys¹⁷⁶ during the catalytic cycle (before reduction by an external thiol) appears structurally plausible and would not involve significant conformational rearrangements (see Fig. 4B). A possible scenario could be the attack of the Cys⁶¹-Cys¹⁷⁴ by the sulfhydryl group of Cys¹⁷⁶ to form a Cys¹⁷⁴-Cys¹⁷⁶ disulfide (as illustrated schematically in Fig. 6B), thus releasing helix α 1 from its (likely energetically unfavorable) state seen in the intermediate structure to the initial (more favorable) position seen in other peroxiredoxins (Fig. 4A). As a consequence, the disulfide would now be located in the flexible C-terminal arm of a single monomer, free to move and highly exposed for subsequent reduction by an external thiol. Indeed, such flexibility does occur in MtAhpC_{C176S}, where the last 25 residues (including the residues at positions 174 and 176) are disordered in two of the three crystallographic independent monomers. Moreover, a mobile C-terminal arm carrying the disulfide bridge could facilitate the interaction of MtAhpC with distinct redox partners *in vivo*, a hypothesis recently put forward from biochemical data showing that, besides AhpD, *M. tuberculosis* thioredoxin C can also efficiently reduce MtAhpC (18).

In apparent conflict with the above hypothesis, Koshkin *et al.*

(21) observed that the C174S and C176S mutants (but not C61S) of MtAhpC could be trapped as covalent intermediates with AhpD, leading these authors to suggest that formation of a disulfide cross-link between Cys⁶¹ and AhpD-Cys¹³³³ is a key step in MtAhpC reduction. However, the substitution of the peroxidatic cysteine (C61S) necessarily precludes the initial peroxide reduction and presumably all downstream electron transfer events, which may thus explain the absence of a covalent intermediate for this mutant without the need to invoke a direct involvement of Cys⁶¹ in the interaction. On the other hand, the partial interchangeability of Cys¹⁷⁴ and Cys¹⁷⁶ as resolving cysteines might explain the formation of covalent adducts for the corresponding point mutants, C174S and C176S.

Interestingly, the peroxidase system composed by NADH, lipoamide dehydrogenase, lipoamide, AhpD, and MtAhpC revealed an atypical kinetics (starting with a lag phase) upon the oxidative activation by *tert*-butyl hydroperoxide as substrate (18). This lag phase was observed to disappear when MtAhpC and AhpD were preincubated with substrate before adding the other components of the reaction, strongly suggesting that the interaction between the first two proteins involves redox-dependent conformational changes. However, no significant structural rearrangements were observed between the oxidized and reduced forms of the AhpD trimer (17). The above observations are therefore consistent with the hypothesis of a mobile C-terminal arm of MtAhpC, which could bring the Cys¹⁷⁴-Cys¹⁷⁶ disulfide into direct contact with the thiol group of Cys¹³³³ at the bottom of the AhpD active site cleft (17, 37) and account in this way for the atypical kinetics.

Conclusions—The crystal structure of MtAhpC_{C176S}, trapped in an intermediate state of the catalytic cycle, displays an unusual 12-mer arrangement instead of the commonly observed 10-mer form of reduced peroxiredoxins. The intramolecular condensation reaction following peroxide reduction entails an unusual rigid-body movement of the entire α -helix containing the peroxidatic cysteine, which creates a transient cavity during the catalytic cycle that might be exploitable for drug design purposes. Based on the structural information, alternative reaction mechanisms can be proposed to account for the sequential reduction of MtAhpC by its redox partner(s) in mycobacterial peroxidase systems.

Acknowledgments—We thank G. Pehau-Arnaudet (Institut Pasteur) and M. Malfois (European Synchrotron Radiation Facility, Grenoble) for technical help with the electron microscopy and small-angle x-ray scattering experiments, respectively.

REFERENCES

- Nathan, C., and Shiloh, M. U. (2000) *Proc. Natl. Acad. Sci. U. S. A.* **97**, 8841–8848
- Sherman, D. R., Sabo, P. J., Hickey, M. J., Arain, T. M., Mahairas, G. G., Yuan, Y., Barry, C. E., III, and Stover, C. K. (1995) *Proc. Natl. Acad. Sci. U. S. A.* **92**, 6625–6629
- Zhang, Y., Dhandayuthapani, S., and Deretic, V. (1996) *Proc. Natl. Acad. Sci. U. S. A.* **93**, 13212–13216
- Slayden, R. A., and Barry, C. E., III (2000) *Microbes Infect.* **2**, 659–669
- Rozwarski, D. A., Grant, G. A., Barton, D. H. R., Jacobs, W. R., and Sacchettini, J. C. (1998) *Science* **279**, 98–102
- Zhang, Y., Heym, B., Allen, B., Young, D., and Cole, S. T. (1992) *Nature* **358**, 591–593
- Heym, B., Alzari, P. M., Honore, N., and Cole, S. T. (1995) *Mol. Microbiol.* **15**, 235–245
- Wengenack, N. L., and Rusnak, F. (2001) *Biochemistry* **40**, 8990–8996
- Manca, C., Paul, S., Barry, C. E., III, Freedman, V. H., and Kaplan, G. (1999) *Infect. Immun.* **67**, 74–79
- Sherman, D. R., Mdluli, K., Hickey, M. J., Arain, T. M., Morris, S. L., Barry, C. E., III, and Stover, C. K. (1996) *Science* **272**, 1641–1643
- Wilson, M., DeRisi, J., Kristensen, H. H., Imboden, P., Rane, S., Brown, P. O., and Schoolnik, G. K. (1999) *Proc. Natl. Acad. Sci. U. S. A.* **96**, 12833–12838
- Hoffmann, B., Hecht, H. J., and Flohé, L. (2002) *Biol. Chem.* **383**, 347–364
- Wood, Z. A., Schröder, E., Harris, J. R., and Poole, L. B. (2003) *Trends Biochem. Sci.* **28**, 32–40
- Chen, L., Xie, Q., and Nathan, C. (1998) *Mol. Cell* **1**, 795–805
- Master, S. S., Springer, B., Sander, P., Boettger, E. C., Deretic, V., and Timmins, G. S. (2002) *Microbiology* **148**, 3139–3144

16. Bryk, R., Griffin, P., and Nathan, C. (2000) *Nature* **407**, 211–215
17. Bryk, R., Lima, C. D., Erdjument-Bromage, H., Tempst, P., and Nathan, C. (2002) *Science* **295**, 1073–1077
18. Jaeger, T., Budde, H., Flohé, L., Menge, U., Singh, M., Trujillo, M., and Radi, R. (2004) *Arch. Biochem. Biophys.* **432**, 182–191
19. Hillas, P. J., Soto del Alba, F., Oyarzabal, J., Wilks, A., and Ortiz de Montellano, P. R. (2000) *J. Biol. Chem.* **275**, 18801–18809
20. Chauhan, R., and Mande, S. C. (2002) *Biochem. J.* **367**, 255–261
21. Koshkin, A., Knudsen, G. M., and Ortiz de Montellano, P. R. (2004) *Arch. Biochem. Biophys.* **427**, 41–47
22. Ellis, H. R., and Poole, L. B. (1997) *Biochemistry* **36**, 13349–13356
23. Van Duyn, G. D., Standaert, R. F., Karplus, P. A., Schreiber, S. L., and Clardy, J. (1993) *J. Mol. Biol.* **229**, 105–124
24. Collaborative Computational Project Number 4 (1994) *Acta Crystallogr. Sect. D* **50**, 760–763
25. Bricogne, G., Vonnrhein, C., Flensburg, C., Schiltz, M., and Paciorek, W. (2003) *Acta Crystallogr. Sect. D* **59**, 2023–2030
26. Jones, T. A., Zhou, J. Y., Cowan, S. W., and Kjeldgaard, M. (1991) *Acta Crystallogr. Sect. A* **47**, 110–119
27. Murshudov, G. N., Vagin, A. A., Lebedev, A., Wilson, K. S., and Dodson, E. J. (1999) *Acta Crystallogr. Sect. D* **55**, 247–255
28. Perrakis, A., Morris, R. M., and Lamzin, V. S. (1999) *Nat. Struct. Biol.* **6**, 458–463
29. Laskowski, R. A., MacArthur, M. W., Moss, D. S., and Thornton, J. M. (1993) *J. Appl. Crystallogr.* **26**, 283–291
30. Alphey, M. S., Bond, C. S., Tetaud, E., Fairlamb, A. H., and Hunter, W. N. (2000) *J. Mol. Biol.* **300**, 903–916
31. Wood, Z. A., Poole, L. B., Hantgan, R. R., and Karplus, P. A. (2002) *Biochemistry* **41**, 5493–5504
32. Schroeder, E., Littlechild, J. A., Lebedev, A. A., Errington, N., Vagin, A. A., and Isupov, M. N. (2000) *Structure* **8**, 605–615
33. Chauhan, R., and Mande, S. C. (2001) *Biochem. J.* **354**, 209–215
34. Hirotsu, S., Abe, Y., Okada, K., Nagahara, N., Hori, H., Nishino, T., and Hakoshima, T. (1999) *Proc. Natl. Acad. Sci. U. S. A.* **96**, 12333–12338
35. Choi, H. J., Kang, S. W., Yang, C. H., Rhee, S. G., and Ryu, S. E. (1998) *Nat. Struct. Biol.* **5**, 400–406
36. Koshkin, A., Zhou, X., Kraus, C. N., Brenner, J. M., Bandyopadhyay, P., Kuntz, I. D., Barry, C. E., III, and Ortiz de Montellano, P. R. (2004) *Antimicrob. Agents Chemother.* **48**, 2424–2430
37. Nunn, C. M., Djordjevic, S., Hillas, P. J., Nishida, C. R., and Ortiz de Montellano, P. R. (2002) *J. Biol. Chem.* **277**, 20033–20040
38. Kraulis, P. J. (1991) *J. Appl. Crystallogr.* **24**, 946–950
39. Merritt, E. A., and Murphy, M. E. P. (1994) *Acta Crystallogr. Sect. D* **50**, 869–873